ELSEVIER

Journal of Alloys and Compounds 271–273 (1998) 128–132

Journal of ALLOYS AND COMPOUNDS

Electronic structures of actinyl nitrate–triethyl phosphate complexes using the DV–DS method

Masaru Hirata[a,*], Rika Sekine[b], Jun Onoe[c], Hirohide Nakamatsu[d], Takeshi Mukoyama[d], Kazuo Takeuchi[c], Shoichi Tachimori[a]

[a] *Japan Atomic Energy Research Institute, Tokai, Naka-gun, Ibaraki 319-11, Japan*
[b] *Dept. of Chemistry, Shizuoka Univ., 836 Ohya, Shizuoka 422, Japan*
[c] *The Institute of Physical and Chemical Research (RIKEN), 2–1 Hirosawa, Wako, Saitama 351-01, Japan*
[d] *Institute for Chemical Research, Kyoto Univ., Uji, Kyoto 611, Japan*

Abstract

Electronic structures of actinyl nitrate–triethyl phosphate complexes ($AnO_2(NO_3)_2 \cdot 2TEP$; An=U, Np, Pu) have been studied, using the relativistic discrete–variational Dirac–Slater molecular orbital method. On the extraction behavior of hexavalent actinyl nitrates, it is known that the distribution ratio decreases in the order U>Np>Pu when neutral organophosphorous agents are used as extractants. To elucidate this variation, the bonding nature between the actinide atom and the donor oxygen atom is examined. It is found that the extractability of the organophosphorous agents decrease with decreasing bond overlap population between the actinide atom and the donor oxygen atom of the extractant. © 1998 Elsevier Science S.A.

Keywords: DV–DS method; Actinyl nitrate; Solvent extraction; Electronic structure; $AnO_2(NO_3)_2 \cdot 2TEP$

1. Introduction

Solvent extraction with tributyl phosphate (TBP) has been widely employed for reprocessing of spent nuclear fuel, since this technique can reduce the quantity of actinides in a waste solution [1]. To clarify factors influencing the solvent extraction of the actinides and to develop new extractants for selective extraction of actinides, information on the electronic structures of the actinide–extractant complexes is indispensable. TBP and other organophosphorous compounds for the extraction of UO_2^{2+}, NpO_2^{2+} and PuO_2^{2+} from an aqueous HNO_3 solution show a common tendency to the decreasing distribution coefficients, $D(UO_2^{2+}) > D(NpO_2^{2+}) > D(PuO_2^{2+})$, as shown in Table 1 [2]. To elucidate this tendency, the chemical bonding nature between the actinide atom and the donor oxygen in the actinyl nitrate–extractant complexes is informative. In the present study, we examine bonding characteristics in the $UO_2(NO_3)_2 \cdot 2H_2O$ and $UO_2(NO_3)_2 \cdot 2TEP$ complexes to compare the ligands in respect to the stability of these compounds, using the discrete variational Dirac–Slater (DV–DS) method. Furthermore, when uranium of the $UO_2(NO_3)_2 \cdot 2TEP$ complex is replaced with neptunium or plutonium, variation of covalent bonding components of the actinide atoms are studied. In the previous study [3], we applied the relativistic DV–DS method to a study of the electronic structure of uranyl nitrate dihydrate. It has been proven that the method provides a theoretical spectrum in good agreement with an experimental X-ray photoelectron spectrum.

In Section 2, cluster models for the complexes and computational procedures are briefly described. In the subsequent section, results of the calculations on the electronic structures for $UO_2(NO_3)_2 \cdot 2H_2O$ and $UO_2(NO_3)_2 \cdot 2TEP$ are presented. It is explained that bonding nature corresponds to the stability of $AnO_2(NO_3)_2 \cdot 2TEP$ complexes.

2. Cluster models and computational method

We took a neutral $UO_2(NO_3)_2 \cdot 2H_2O$ complex with D_{2h} symmetry [4,5] and $AnO_2(NO_3)_2 \cdot 2TEP$ (where An=U, Np and Pu) with C_{2v} symmetry [6–8]. The structures of $UO_2(NO_3)_2 \cdot 2H_2O$ and $UO_2(NO_3)_2 \cdot 2TEP$ are shown in

*Corresponding author. Tel.: 00 81 29 282 6256; fax: 00 81 29 282 6723; e-mail: hirata@popsvr.tokai.jaeri.go.jp

0925-8388/98/$19.00
PII: S0925-8388(98)00039-5

Table 1
Distribution ratio for extraction of actinyl ions with different trialkyl phosphates (1.09 M in dodecane, 3.0 M HNO_3, 30°C)

Extractant	D (UO_2^{2+})	D (NpO_2^{2+})	D (PuO_2^{2+})
TBP(tri-*n*-butyl phosphate)	25	15.6	3.5
Triisobutyl phosphate	22	15.9	3.4
Tri-*n*-pentyl phosphate	32	19.3	4.1
Triisopentyl phosphate	34	18.9	4.4
Tri-3-phentyl phosphate	49	22	5.0
Tris(3-methyl-2-pentyl) phosphate	47	25	5.4
Tri-*n*-hexyl phosphate	38	20.0	4.5
Tris(4-methyl-2-pentyl) phosphate	38	24	4.9
Tri-*n*-octyl phosphate	33	15.7	3.9
Tris(2-ethylhexyl) phosphate	58	23	5.7

Figs. 1 and 2, respectively. The atomic positions of $UO_2(NO_3)_2{\cdot}2H_2O$ were taken from X-ray and neutron diffraction data. For the calculation of $UO_2(NO_3)_2{\cdot}2TEP$, U-O (of TEP) and O=P bond lengths were taken from X-ray diffraction data [4,5]. The atomic positions of the ethyl groups were taken from a structure of TEP optimized by MNDO-PM3 method [9,10]. The interatomic distances between Np, Pu and O of TEP were estimated on the basis of the ratio of ionic radius for these hexavalent actinide ions [11,12].

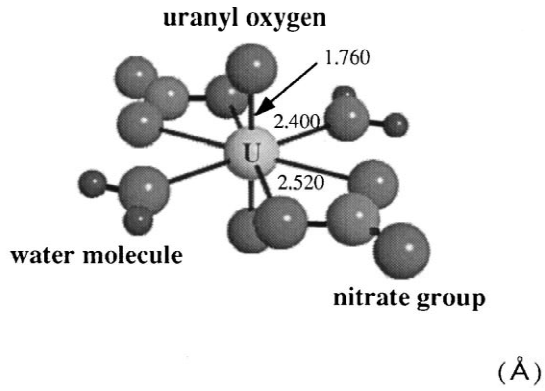

Fig. 1. Cluster model of $UO_2(NO_3)_2{\cdot}2H_2O$.

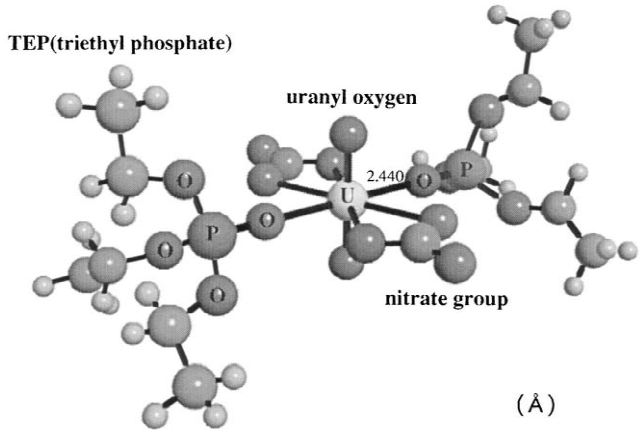

Fig. 2. Cluster model of $UO_2(NO_3)_2{\cdot}2TEP$.

The one-electron molecular Hamiltonian for the Dirac–Slater MO method is written as:

$$H = c\alpha P + \beta mc^2 + V(r) \quad (1)$$

where c, P, m, α, β and $V(r)$ denote the velocity of light, the operator of momentum, the rest mass of electron, the Dirac matrices and the sum of coulomb and exchange potentials, respectively.

The molecular wave functions were expressed as linear combinations of atomic orbitals obtained by numerically solving the Dirac–Slater equations in the atomic-like potential which was derived from a spherical average of the molecular charge density around each corresponding nucleus. Thus the atomic orbitals, which are employed as basis functions, were automatically optimized for the molecule [13]. Since the spin function is included in the relativistic Dirac equation, D_{2h} and C_{2v} symmetries reduce to D^*_{2h} and C^*_{2v} double point groups, respectively. Symmetry orbitals which produce irreducible representations for the D^*_{2h} and C^*_{2v} symmetry were constructed with the atomic orbitals by the projection operator method [14,15].

Two-center charge densities are partitioned into one-center (atomic) charges by means of the Mulliken population analysis [16] in the self-consistent charge (SCC) method [17], which was used to approximate the self-consistent field. The computational details of the DV–DS method used in the present work have been described elsewhere [18,19]. According to the population analysis, the bond overlap population $P_B(k, l)$ between the k-th and l-th atoms is defined by:

$$P_B(k, l) = \sum_i \sum_{r,s} 2N(i)C^k_{ir}C^l_{is}\langle\phi^k_r|\phi^l_s\rangle \quad (2)$$

In Eq. (2), $N(i)$ denotes the occupation number of electrons in the i-th MO. The quantities C^k_{ir} and C^l_{is} represent the coefficients of normalized atomic orbitals ϕ^k_r and ϕ^l_s of the k-th and l-th atoms, respectively, in the linear combination of these atomic orbitals for the i-th MO. The P_B value is a good indicator of the strength of the covalent bond [20,21]. Since the Mulliken populations depend on the choice of basis-set sizes to a certain extent, we used the

same basis-set size (U, Np, Pu1s-7p, P 1s-3p, O, N, C 1s-2p, H 1s) for all the calculations.

The DV–DS calculations were performed with the Slater exchange parameter α of 0.7 and with 20 000 DV sample points for $UO_2(NO_3)_2 \cdot 2H_2O$ and 40 000 DV points for $UO_2(NO_3)_2 \cdot 2TEP$. The calculations were carried out self-consistently until the difference in orbital populations between the initial and final stages of the iteration was less than 0.01.

3. Results and discussion

Fig. 3 shows the energy level structures around the HOMO and LUMO levels of $UO_2(NO_3)_2 \cdot 2H_2O$ and $UO_2(NO_3)_2 \cdot 2TEP$. The energy gap between HOMO and LUMO is found to be 1.60 eV for $UO_2(NO_3)_2 \cdot 2H_2O$ and 1.72 eV for $UO_2(NO_3)_2 \cdot 2TEP$, respectively. As shown in Fig. 3 as well, the main component of HOMO for each compound is the O 2p orbitals of nitrate groups, while LUMO mainly involves the U 5f orbitals.

The arrows in Fig. 3 indicate the MOs which contain O 2p of donor oxygen in the ligands, i.e., $O=PO_3$ and OH_2. The O 2p components of $O=PO_3$ spread over the upper valence levels compared with those of the water molecules. Therefore, these MO levels characterize the difference in bond nature between $UO_2(NO_3)_2 \cdot 2H_2O$ and $UO_2(NO_3)_2 \cdot 2TEP$.

To elucidate the contribution of the orbital components to the valence levels in a wider energy range, we plotted the partial density of states (pDOS) for atomic orbital components and energy dependence of the bond overlap population (P_B) as shown in Fig. 4, where the levels were replaced with Lorentzian curves to clarify the density and distribution of levels. The significant difference in pDOS is the O 2p contribution of the ligands in the occupied states and the U 5f states in the unoccupied states. In the case of $UO_2(NO_3)_2 \cdot 2TEP$, the partial density of the O 2p states increase below the HOMO level, while the U 5f orbitals in the unoccupied states decrease by replacing the water molecule with TEP. The bond overlap population plots reveal that the bonding interaction is mainly due to the MO's in the range of $-10 \sim -15$ eV. The antibonding states are predominant around the HOMO level and decrease by the replacement of the water molecule with TEP.

Table 2 shows the orbital populations, effective charges and P_B for $UO_2(NO_3)_2 \cdot 2H_2O$ and $AnO_2(NO_3)_2 \cdot 2TEP$ (An=U, Np, Pu). The bond strength in the TEP complex is discussed through comparing the results between $UO_2(NO_3)_2 \cdot 2H_2O$ and $UO_2(NO_3)_2 \cdot 2TEP$. The absolute values of the effective charges on the U and O donors in the ligands and P_B between U and O increase on the introduction of TEP. This indicates that both ionic and covalent bonding are strengthened by the complexation with the TEP molecules.

In order to understand the tendency of the distribution ratios, $D(UO_2^{2+}) > D(NpO_2^{2+}) > D(PuO_2^{2+})$, we examine $NpO_2(NO_3)_2 \cdot 2TEP$ and $PuO_2(NO_3)_2 \cdot 2TEP$ as well. When the complexes in the solution have the solvent and the ligand in common and their structures are very similar, the principal factor changing the $D(AnO_2^{2+})$ values is attributed to the bond nature between An and the donor O of the ligand. As shown in Table 2, the orbital population of An 5f increases from 2.864 to 5.023, while the An 6d, 7s and 7p populations slightly decrease with increasing the atomic number. The effective charges of the actinides decrease in the order of U>Np>Pu. However, the abso-

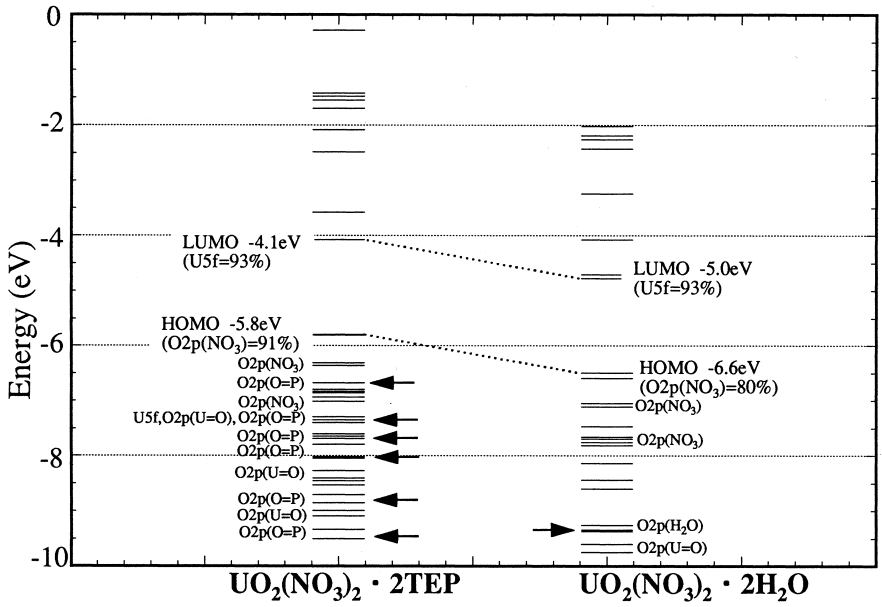

Fig. 3. Valence energy level structures of $UO_2(NO_3)_2 \cdot 2TEP$ and $UO_2(NO_3)_2 \cdot 2H_2O$.

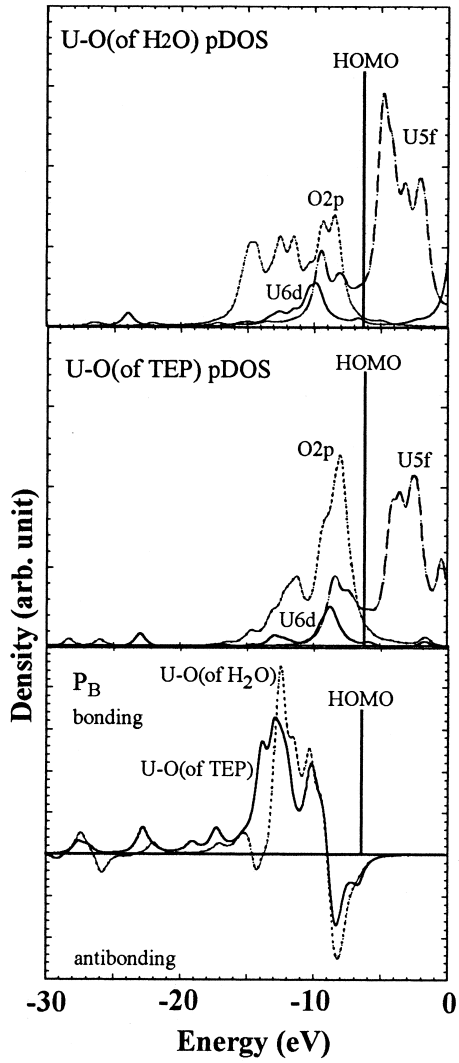

Fig. 4. Partial density of states and bond overlap population plots for $UO_2(NO_3)_2 \cdot 2H_2O$ and $UO_2(NO_3)_2 \cdot 2(TEP)$.

lute values of the effective charges on the oxygen atoms of the ligands increase. The substantial change in the bond nature of $AnO_2(NO_3)_2 \cdot 2TEP$ appears in a decrease of the P_B value with increasing atomic number of actinides. Thus, the decrease in the covalency makes $PuO_2(NO_3)_2 \cdot 2TEP$ less stable than the uranyl complex. This decrease of P_B corresponds to the decreasing tendency of the distribution ratios for the hexavalent actinides extraction system.

4. Notation

Coordination chemistry: organometallics

References

[1] K.L. Nash, G.R. Choppin (Eds.), Separation of f Elements, Plenum Press, NY, 1995.
[2] Z. Kolarik, Behavior of transuranium elements in the PUREX process in: A.J. Freeman, C. Keller (Eds.), Handbook on the Physics and Chemistry of the Actinides, Elsevier Science Publishers B.V., 1991.
[3] M. Hirata, H. Monjyushiro, R. Sekine, J. Onoe, H. Nakamatsu, T. Mukoyama, H. Adachi, K. Takeuchi, J. Electron Spectrosc. Relat. Phenom. 83 (1997) 59.
[4] J.C. Taylor, M.H. Mueller, Acta Cryst. 19 (1965) 536.
[5] N.K. Dalley, M.H. Mueller, S.H. Simonsen, Inorg. Chem. 10 (1971) 323.
[6] B. Kanellakopulos, E. Dornberger, R. Maier, B. Nuber, H.-G. Stammler, M.L. Ziegler, Z. Anorg. Allg. Chem. 619 (1993) 593.
[7] J.E. Fleming, H. Lynton, Chem. Ind. (1959) 1409.
[8] J.E. Fleming and H. Lynton, Chem. and Ind. (1960) 1415.
[9] J.J.P. Stewart, J. Comput. Chem. 10 (1989) 209.
[10] J.J.P. Stewart, J. Comput. Chem. 10 (1989) 221.
[11] Yu.F. Volkov, I.I. Kapshukov, Radiokhimiya 18 (1976) 284.

Table 2
Orbital populations, effective charges and bond overlap population (P_B)

	$UO_2(NO_3)_2 \cdot 2H_2O$	$UO_2(NO_3)_2 \cdot 2TEP$	$NpO_2(NO_3)_2 \cdot 2TEP$	$PuO_2(NO_3)_2 \cdot 2TEP$
An5f	2.935	2.864	3.936	5.023
An6d	1.992	1.919	1.876	1.793
An7s	0.190	0.174	0.165	0.157
An7p	0.259	0.275	0.251	0.229
Effective charge	+0.890	+1.034	+1.002	+0.997
O2s(H_2O, TEP)	1.747	1.759	1.751	1.762
O2p(H_2O, TEP)	4.644	4.718	4.729	4.730
Effective charge	−0.392	−0.477	−0.481	−0.491
Bond overlap population (P_B) U-O(H_2O, TEP)	0.417	0.651	0.629	0.599

[12] R.D. Shannon, Acta Cryst. A32 (1976) 751.
[13] H. Adachi, M. Tsukada, C. Satoko, J. Phys. Soc. Jpn. 45 (1978) 875.
[14] J. Meyer, W.D. Sepp, B. Fricke, A. Rosen, Computer Phys. Commun. 54 (1989) 55.
[15] J. Meyer, W.D. Sepp, B. Fricke, A. Rosen, Computer Phys. Commun. 96 (1996) 263.
[16] R.S. Mulliken, J. Chem. Phys. 23 (1955) 1833, 1841, 2338, 2343.
[17] A. Rosen, D.E. Ellis, H. Adachi, F.W. Averill, J. Chem. Phys. 65 (1976) 3629.
[18] A. Rosen, D.E. Ellis, J. Chem. Phys. 62 (1975) 3039.
[19] H. Nakamatsu, H. Adachi, T. Mukoyama, Bull. Inst. Chem. Res. Kyoto. Univ. 70 (1992) 16.
[20] J. Onoe, H. Nakamatsu, T. Mukoyama, R. Sekine, H. Adachi, K. Takeuchi, Inorg. Chem. 36 (1997) 1934.
[21] J. Onoe, K. Takeuchi, H. Nakamatsu, T. Mukoyama, R. Sekine, B.-II. Kim, H. Adachi, J. Chem. Phys. 99 (1993) 6810.